Properties of Snowflake Diverted H-Mode Plasmas in TCV

B. Labit, G. Canal, H. Reimerdes, B. Tal[1], W. Vijvers, S. Coda, B.P. Duval,
T. Morgan[2], G. De Temmerman[2], J. Zielinski[2] and the TCV team

École Polytechnique Fédérale de Lausanne (EPFL), Centre de Recherches en Physique des Plasmas (CRPP), Association EURATOM-Confédération Suisse, CH-1015 Lausanne, Switzerland. [1]*Institute for Particle and Nuclear Physics, Wigner Research Centre for Physics, Hungarian Academy of Sciences, EURATOM Association, Budapest, Hungary.* [2]*Dutch Institute for Fundamental Energy Research (DIFFER), Association EURATOM-FOM, Nieuwegein, The Netherlands.*

The snowflake (SF) divertor [1, 2] is an innovative solution to reduce plasma-wall interactions by acting on the magnetic field topology. In this configuration, both the poloidal magnetic field and its spatial first derivatives vanish at the null point. The separatrix divides the poloidal plane in six regions and, as a consequence, the configuration has four divertor legs. The properties of the SF divertor geometry are expected to affect the local heat loads on the divertor plates, in particular in H-mode and during Edge Localized Modes (ELMs) [3]. In TCV, the degree of proximity to a true SF divertor configuration is parametrized by the parameter σ, which is the ratio of the distance between the two X-points to the minor radius of the plasma. It has been demonstrated that single-null (SN) (σ=2.7) and SF (σ=0.4) configurations have a similar H-mode power threshold, whereas the SF confinement is 15% higher [4]. The most striking difference is for type-I ELMs: their frequency is reduced by a factor 2-3 with the SF divertor, while the ratio of the energy lost per ELM to the plasma energy is only increased by 20-30%. To investigate the properties of the SF divertor in H-mode plasmas, a scan in the σ parameter is performed on TCV on a shot to shot basis. Typical discharge parameters are: I_p = 300 kA, B_t = 1.45 T, κ_{95} = 1.7, δ_{95} = 0.2, q_{95} = 2.6, ECRH: 2 $\times$ 450 kW (X3) + 450 kW (X2). Some plasma parameters, averaged over the steady phase $0.6 \leq t \leq 1$ s are shown in Fig. 1a). The ELM regime for σ >1 is undoubtedly type-I, while for the lowest σ values (0.4 and 0.8) the ELMs show characteristics of type-III (smaller $\Delta W/W$, higher f_{ELM}, lower confinement). A possible explanation for this transition is the slightly lower absorbed ECRH power for these two shots, combined with an earlier L-H transition. Future experiments within a single ELM regime will have to be performed at higher ECH power, well above the L-H transition threshold. Heat and particle loads are monitored in the vicinity of strike points 1, 2 and 3 with Langmuir probes operated at a constant negative voltage, measuring J_{sat}. Complementary to this diagnostic, an array of 7 pinhole cameras, based on fast (200 kHz) AXUV diodes, has recently been refurbished (140 chords covering the poloidal cross-section, as shown in Fig. 1b)). These diodes are sensitive to photons in the range 1 eV-10 keV (1 μm-0.1 nm), but have

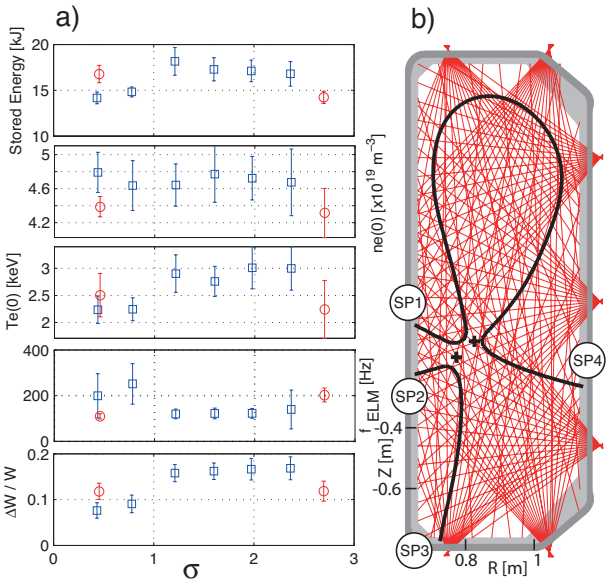

Figure 1: *a) Time averaged plasma parameters for the shot to shot σ scan (blue □) and for #39874 from [4] (red ○). b) TCV cross-section with the 140 AXUV lines of sight (red) and the separatrix (thick black) of a SF plasma.*

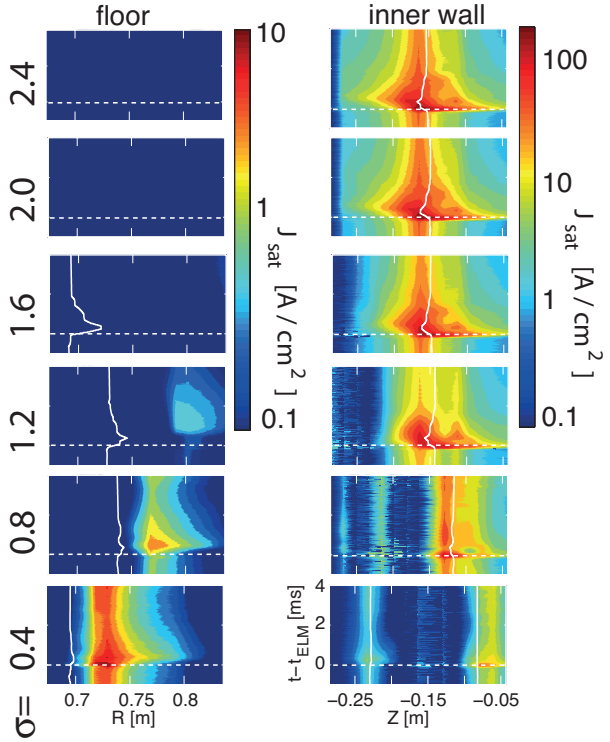

Figure 2: *Ensemble averaged J_{sat} over an ELM cycle measured by LPs on the floor (left) and on the inner wall (right) for various σ. The white lines show the strike point position during an ELM. The horizontal dashed line indicates the ELM crash.*

uneven spectral response and cannot provide the absolute radiated power during an ELM. However they can supply information on the distribution of radiation during the ELM cycle [5]. For each shot, ELMs are detected as peaks in the D_α signal in the period $0.6 \leq t \leq 1$ s. The saturation current density J_{sat} and the line integrated radiated power are ensemble averaged over the ELM cycle ($-1 \leq t - t_{ELM} \leq 4$ ms).

The results for Langmuir probe measurements are summarized in Fig. 2. The srike point positions are extracted from the reconstruction of the magnetic equilibrium around one ELM for each shot with a temporal resolution of 0.2 ms. For large σ, it is suggested that the strike points are moving over distances comparable to the probe separation (about 1 cm), consistent with the measured J_{sat} profiles. It has to be noted that σ is reduced by 10% at the ELM crash. The shape of the J_{sat} profile measured on the floor indicates that the radial position of SP3 is not well reconstructed by LIUQE, probably because of a systematic offset in the poloidal field coils measurements. As σ is decreased, the current measured at the ELM crash around SP1 reduces from ∼200 to ∼50 A/m^2, in line with previously reported results [6]. Particle fluxes start to be detected at SP3 for σ<1.5, and at the smallest X-point separation, J_{sat} at SP3 and at SP2 are of the same order of magnitude (∼ 10 A/m^2). For σ ∼ 0.4, the total particle flux reaching SP3, integrated over both the ELM cycle and the wetted area, is about 30% of the total flux reaching SP1. This is a clear indication that particle and heat fluxes ejected from the

plasma core during ELMs are redistributed over the 4 divertor legs of the snowflake divertor. For σ=1.2 and σ=0.8, a delay of 0.5-1 ms with respect to the ELM crash is observed for the particle flux at SP3. This delay is consistent with particles travelling along the approximately 40 m long magnetic field lines between the divertor entrance and the strike point on the floor at an ion sound speed of about 10^5 m.s^{-1} ($T_e \sim 150$ eV at the separatrix).

A tomographic inversion of the ensemble averaged line-integrated radiation measured by the AXUV photodiodes is performed on a 2×2 cm square pixels grid covering the entire TCV cross-section. Results are summarized in Fig. 3. For any X-points separation, the radiated power before the ELM is of the same magnitude and is localized in between the divertor entrance and SP1. At the ELM crash, most of the radiated power density is localized at the main strike points (SP1 and SP4), except for the lowest σ value. In this case, SP2 and SP3 are clearly activated and little radiation is visible at SP4. Moreover, although this diagnostic cannot provide a calibrated radiated power density P_{rad}, if we assume an average conversion coefficient of 0.24 A/W, we found that the ratio of the average total radiated energy during ELMs (P_{rad} integrated over the entire TCV volume and ELM cycle duration) to the loss of stored energy ΔW_{ELM} is doubled for $\sigma \leq 1$ compared to σ>1 (not shown).

The shot #43454 is an ELMy H-mode in which the separation between both X-points is progressively decreased (Fig. 4a)). Heat loads on the divertor targets around SP1 and SP3 are monitored with two fast framing infrared cameras. One camera (framing rate: 13 kfps), looking at the inner wall from an equatorial port, measures an uncalibrated tile temperature while the other one (15 kfps) is looking at the machine floor from a top port and provides calibrated tile temperatures. The heat flux is extracted from a modeling of the tile temperature [7]. Figure 4c-d) shows the heat loads on the divertor targets during ELMs in the SN and the SF configurations. IR measurements on the floor shows that SP3 starts to be active for $\sigma \leq 0.6$ and the heat load peaks at about 10 MW/m^2. In the vicinity of SP1, the uncalibrated tile temperature is reduced by a factor of four at the ELM crash, when moving from the SN to the SF divertor. This is consistent with the particle flux reduction observed with the Langmuir probes. For each ELM in the SN phase (0.7 $\leq$t$\leq$0.9 s) and in the SF phase (1.4 $\leq$t$\leq$1.6 s), the experimental heat flux profile is fitted with the convolution of a gaussian profile of width S and an exponential profile of decay length λ_q as proposed by Eich *et al.* [8]. Examples of fits are shown in Fig. 4e) and the average fitted parameters are reported in Fig. 4f). The integral power decay width $\lambda_{\text{int}} \equiv \int [q(s) - q_{BG}]\, ds/(q_{max} - q_{BG})$ relates the peak heat load on the divertor target to power deposited at this place. At SP1, even if the heat flux profile tends to be more asymmetric in the SF phase, λ_{int} ($\sim$ 1 cm) and λ_q ($\sim$ 0.5 cm) do not change notably between both divertor con-

figurations. At SP3, the heat loads are more symmetric with respect to the strike point position ($S > \lambda_q$). This suggests a strong perpendicular diffusion possibly compatible with the model of intense plasma convection around the null-point during ELMs proposed by Ryutov *et al.* [3]. By coincidence, λ_{int} is of the same order of magnitude for this additionnal strike point as for SP1. Our understanding of the snowflake divertor physics will progress with the additional informations provided by the new array of probes currently under installation which covers the target zone of SP4 together with a heated tile on the inner wall for calibrated thermography.

The authors are thanking their colleagues from LLNL in particular D. D. Ryutov for fruitful discussions. This work is partly funded by the Fonds National Suisse de la Recherche Scientifique and the European Communities under the contract of Association between EURATOM CRPP and EURATOM HAS. The views and opinions expressed herein do not necessarily reflect those of the European Commission.

[1] Ryutov D. D. *et al.*, Phys. Plasmas **15**, 092501 (2008)
[2] Piras F. *et al.*, Plasma Phys. Control. Fusion **51**, 055009 (2009)
[3] Ryutov D. D. *et al.*, Contrib. Plasma Phys. **52**, 539 (2012)
[4] Piras F. *et al.*, Phys. Rev. Lett. **105**, 155003 (2010)
[5] Veres G. *et al.*, J. Nucl. Mat.l **390-391**, 835 (2009)
[6] Labit B. *et al.*, 38 *th* EPS Conference on Plasma Physics, P2.76, Strasbourg, 2011
[7] Herrman A., ECA Vol. 25A, 2109 (2001)
[8] Eich T. *et al.*, Phys. Rev. Lett., **107**, 215001 (2011)

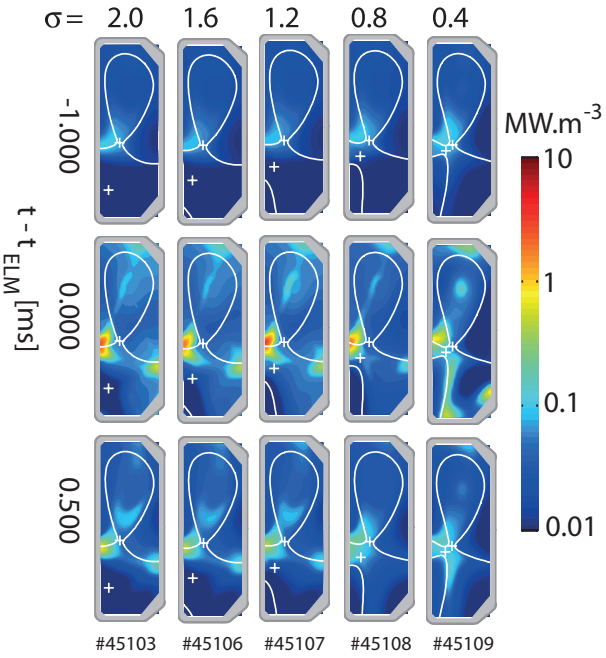

Figure 3: *Radiated power density after tomographic inversion at several times of the ELM cycle.*

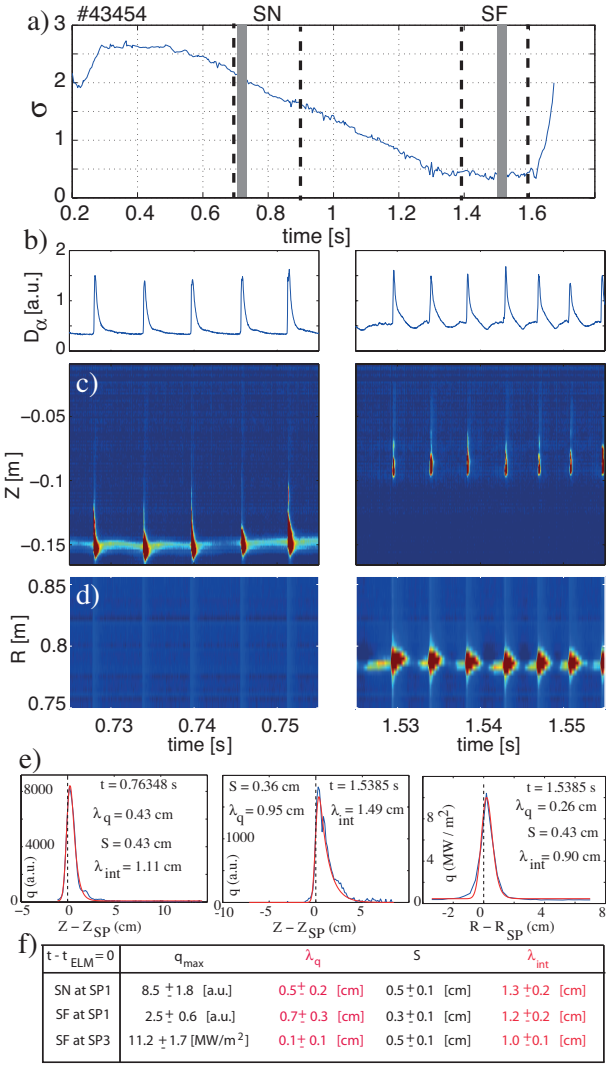

Figure 4: *a) Scan of the σ value during #43454 (ELMy H-mode). b) D_α signal showing ELMs. c) Uncalibrated heat flux around SP1. d) Calibrated heat flux around SP3. e) Example of fits as in [8]. f) Summary of fitted parameters.*